Available online at www.sciencedirect.com

SciVerse ScienceDirect

Ceramics International 39 (2013) 8261–8266

CERAMICS INTERNATIONAL

www.elsevier.com/locate/ceramint

Magnetic properties of Eu^{3+} lightly doped $ZnFe_2O_4$ nanoparticles

Lili Yang[a,b], Zhe Wang[a,b], Bowen Zhai[a], Yexu Shao[a,b], Zhiqiang Zhang[a,b], Yunfei Sun[c], Jinghai Yang[a,b,*]

[a]*Institute of Condensed State Physics, Jilin Normal University, Siping 136000, China*
[b]*Key Laboratory of Functional Materials Physics and Chemistry (Jilin Normal University), Ministry of Education, Siping 136000, China*
[c]*Key Laboratory of Excited State Physics, Changchun Institute of Optics Fine Mechanics and Physics, Chinese Academy of Sciences, Changchun 130033, China*

Received 31 January 2013; received in revised form 2 April 2013; accepted 3 April 2013
Available online 10 April 2013

Abstract

Eu-doped $ZnFe_2O_4$ nanoparticles ($ZnFe_{2-x}Eu_xO_4$ ($x=0$, 0.01, 0.02, 0.03)) with different Eu^{3+} doping concentration were synthesized by a sol–gel method. The nanoparticles were characterized by conventional powder X-ray diffraction, energy dispersive X-ray spectrometry, transmission electron microscopy, X-ray photoelectron spectroscopy and vibrating sample magnetometry. The detailed investigation revealed the $ZnFe_{2-x}Eu_xO_4$ ($x=0$, 0.01, 0.02, 0.03) nanoparticles had zero coercivity with the increasing M/H as the content of Eu^{3+} ions increased. The corresponding magnetic mechanism had been discussed in detail.

Keywords: $ZnFe_2O_4$; Zero coercivity; Magnetization

1. Introduction

To date, one of the most interesting and challenging issues of the science of magnetic nanomaterials is how to optimize their magnetic properties and introduce new optical, electronic or photochemical properties as well [1]. Nanosized magnetic nanoparticles, due to their unique electromagnetic properties of technological importance in the magnetocaloric industries, have attracted intensive attention. Among the wide variety of nanosized magnetic nanoparticles which is susceptible to be modified for manipulating their properties, spinel ferrite nanoparticles are one of the most attractive systems. This is mainly because that the spinel structure is complex and adaptive in comparison with other magnetic nanoparticles (elemental, intermetallic, oxides), which can be modified in various ways to obtain some novel or enhanced physical properties. Therefore, spinel ferrites nanoparticles provide one of the most versatile experimental environments to probe the fundamental and applied behavior of magnetic nanoparticles.

Any candidate magnetocaloric material should have a high saturation magnetization (M_s) and small coercivity [2]. So far, people can achieve these changes by improving the preparation method, adjusting the particle-size, doping or post-processing. According to the previous reports, introducing trivalent rare earth (RE) cations into the inverse ferrite lattice can induce RE^{3+}–Fe^{3+} interactions, which could modify their corresponding magnetic properties [3,4]. Therefore, in this work, the europium (Eu) as Table IVf metal with an ionic radius of 0.107 nm was selected as the doping species [5], which was expected that the introduction of Eu^{3+} into the Fe-lattice would obtain a high M_s. In detail, we would like to present the controllable synthesis of $ZnFe_{2-x}Eu_xO_4$($x=0$, 0.01, 0.02, 0.03) nanoparticles by a sol–gel method. The size dependence of magnetic properties of as-synthesized $ZnFe_{2-x}Eu_xO_4$ was investigated.

2. Experimental

2.1. Synthesis

Eu-doped $ZnFe_2O_4$ nanoparticles were synthesized via the sol–gel method with a post-annealing treatment. For $ZnFe_{2-x}Eu_xO_4$ ($x=0$, 0.01, 0.02, 0.03) nanoparticles, the citric acid (CA),

*Corresponding author at: Institute of Condensed State Physics, Jilin Normal University, Siping 136000, China. Tel.: +86 434 3294566.
E-mail address: jhyang1@jlnu.edu.cn (J. Yang).

0272-8842/$ - see front matter © 2013 Elsevier Ltd and Techna Group S.r.l. All rights reserved.
http://dx.doi.org/10.1016/j.ceramint.2013.04.011

$Zn(NO_3)_2{\bullet}6H_2O$ and $Fe(NO_3)_3{\bullet}9H_2O$ were firstly dissolved in 200 ml deionized water with a molar ratio of 3:1:2. Eu_2O_3 powder was dissolved in dilute nitric acid 0.1 mol/l aqueous solution of europium nitrate. Then the europium nitrate was added into it with a Zn:Eu molar ratio of 1:1, 1:2, 1:3, respectively. The mixture was magnetic stirred for 24 h at the room temperature. After stirring, the solution was kept in a dry cabinet at 80 °C for 48 h to obtain $ZnFe_2O_4$ gel. After that, we adjusted the dry cabinet to 120 °C for puffing 24 h to obtain the xerogel. Herein, we obtained the precursor of the samples. These precursor powders were annealed at 750 °C in air for 2 h to get the final samples. For comparison, we also prepared pure $ZnFe_2O_4$ sample in the similar process only without adding Eu^{3+} solution.

2.2. Characterization

X-ray diffraction (XRD) patterns were recorded by a MAC Science MXP-18 X-ray diffractometer using a Cu target radiation source was used to study the crystal structure and morphology of the samples. The scanning electron microscope (SEM, S-570, Hitachi) with an energy dispersive spectrometer (EDS) was used to characterize the morphology and different chemical composition of the samples. The transmission electron microscope (TEM, JEM-2100, JEOL) spectroscopy system was used to qualitatively confirm the detailed microscopic structure. A quantitative compositional analysis was carried out by using an X-ray photoelectron spectroscopy (XPS) in an ultra-high vacuum chamber at a pressure lower than 1.333×10^{-7} Pa. The magnetic properties of the samples were measured by a Lake Shore 7407 vibrating sample magnetometry (VSM).

3. Results and discussion

Fig. 1 shows the XRD patterns of the $ZnFe_{2-x}Eu_xO_4$ ($x=0$, 0.01, 0.02, 0.03) nanoparticles. For pure $ZnFe_2O_4$, the diffraction peaks at 2θ values of 29.8°, 35.09°, 42.71°, 56.5°, and 62.04° could be ascribed to the reflection of (220), (311), (400), (511) and (440) planes respectively. Its position and relative intensity matched well with the standard patterns of $ZnFe_2O_4$ (JCPDS file no. 22-1012), which indicated that the samples owned spinel structure. For Eu^{3+} doped samples, no diffraction peaks were detected from europium oxides, which indicated the Eu^{3+} ions successfully substituted for Fe^{3+} in $ZnFe_2O_4$ matrix. However, there was an unknown peak between (220) and (311) peaks marked by "*" in the figure, we carefully checked the standard JCPDS card to determine the unknown peak and found that it should be assigned to the Fe_2O_3. This maybe due to the Eu^{3+} ions taking the place of Fe^{3+} ions, which will be further verified by XPS results, so that a few Fe^{3+} ions would be separated out from $ZnFe_2O_4$. However, its influence on the magnetic properties could be ignored since its content was rather low. We also found in Fig. 1 that, with increasing the Eu^{3+} ions content, the diffraction intensities in the XRD patterns decreased and the full width at half maximum (FWHM) broadened step by step, indicating the degeneration of crystalline qualities. The average crystalline size was calculated using the Scherer equation

$$D = \frac{0.89\lambda}{\beta \cos\theta} \quad (1)$$

where D is the crystalline size, λ is the wavelength of the X-ray radiation, θ is the Bragg's angle, and β is the FWHM on 2θ scale. According to Eq. (1), the calculated average crystalline size of $ZnFe_{2-x}Eu_xO_4$ ($x=0$, 0.01, 0.02, 0.03) was 42.32 nm, 25.89 nm, 21.61 nm, 17.82 nm, respectively. Clearly, with increasing the Eu^{3+} ions content, the size of the samples decreased step by step, indicating the incorporation of Eu^{3+} into $ZnFe_2O_4$ restrained the lattice growth [6]. Through calculation using the Lattice Geometry equation, we also obtained the lattice constant of $ZnFe_{2-x}Eu_xO_4$ ($x=0$, 0.01, 0.02, 0.03) was 8.440 Å, 8.445 Å, 8.453 Å, 8.457 Å, respectively [7,8].

We further performed the EDS measurement on the as-prepared $ZnFe_{2-x}Eu_xO_4$ (x=0.01, 0.02, 0.03) nanoparticles to verify the chemical composition, which is shown in the Fig. 2a, b, c. In Fig. 2a, b and c, we could find that, except the Zn, O and Fe elements, a small amount of Eu elements existed in the $ZnFe_{2-x}Eu_xO_4$ ($x=0.01$, 0.02, 0.03) samples. Their corresponding Eu^{3+} quantitative concentration had been estimated to be 0.66%, 0.96%, 1.45%, respectively, which was smaller than the prospected doping concentration. This could be attributed to the large difference of the ionic radius of Fe^{3+} and Eu^{3+} ions.

To qualitatively reveal the detailed microscopic structure, we used TEM technique to characterize the $ZnFe_{1.97}Eu_{0.03}O_4$ sample. Fig. 3a presents its TEM image, which clearly illustrated the samples were uniform in morphology with particle size distribution in the range of 15–20 nm. To make the structure clear, the HRTEM images corresponding to the R1 place marked by the red dot ring in Fig. 3a is shown in Fig. 3b. We clearly saw the fringe lines along at least three directions. The fringe spaces for three directions were all 0.315 nm, which was corresponding to the (220) plane distance of the spinel structure. However, this spacing was bigger than that of standard $ZnFe_2O_4$ (0.298 nm), which was mainly caused by the cell volume expansion when the Eu^{3+} ions doped into $ZnFe_2O_4$ since the ionic radius of Eu^{3+} was

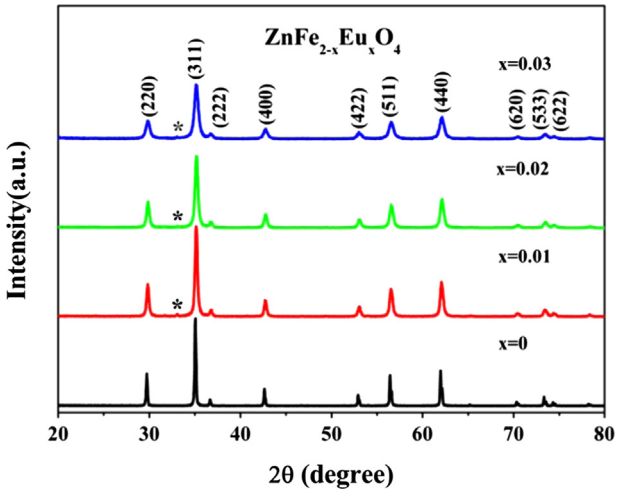

Fig. 1. XRD patterns of $ZnFe_{2-x}Eu_xO_4$ ($0 \le x \le 0.03$) nanoparticles.

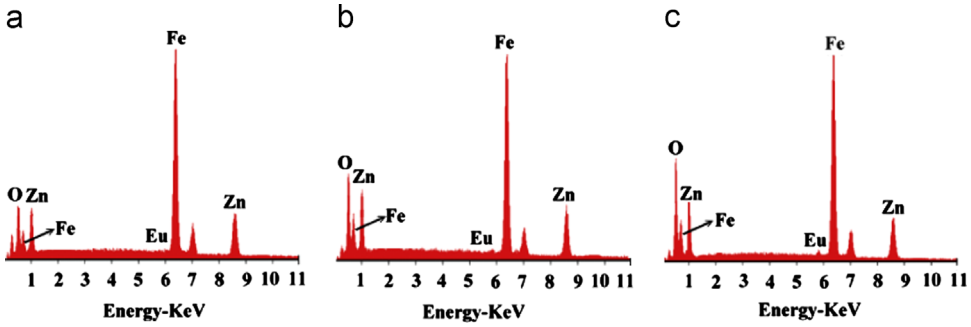

Fig. 2. EDS images of $ZnFe_{2-x}Eu_xO_4$ ($0.01 \leq x \leq 0.03$) nanoparticles.

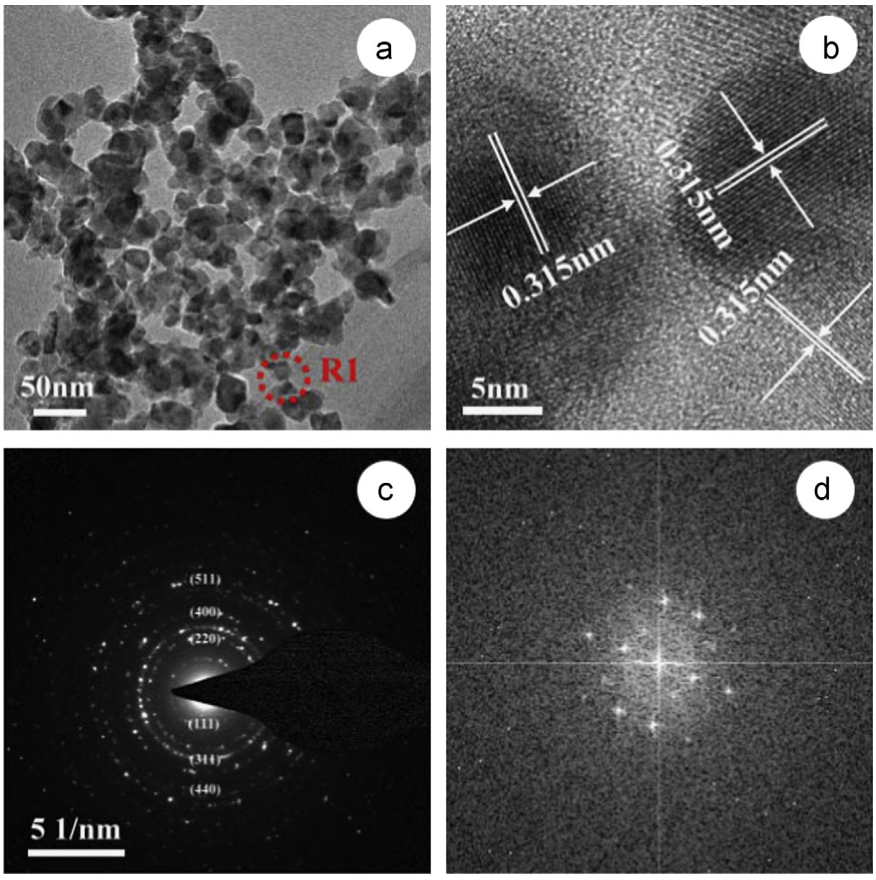

Fig. 3. TEM, HRTEM, SAED and (FFT) images of $ZnFe_{1.97}Eu_{0.03}O_4$ nanoparticles: (a) TEM image; (b) HRTEM image corresponding to the region marked by the red dot ring in (a); (c) SAED images of the $ZnFe_{1.97}Eu_{0.03}O_4$ nanoparticles; (d) FFT images of the $ZnFe_{1.97}Eu_{0.03}O_4$ nanoparticles. (For interpretation of the references to color in this figure legend, the reader is referred to the web version of this article.)

much bigger than that of Fe^{3+}. Fig. 3c shows the corresponding selected area electron diffraction (SAED) of the sample. The diffraction pattern indicated the polycrystalline nature of the sample, it could be further confirmed that the nanoparticles was the spinel structure, which was in agreement with the XRD analysis. The FFT image (Fig. 3d) further proved the result of SAED, in which the few streaky spots might come from the defects in the lattice.

To further investigate the chemical compositions and the bonding states, we performed XPS measurements on the $ZnFe_{1.97}Eu_{0.03}O_4$ sample. Prior to the XPS measurements, the sample was cleaned by sputtering with an Ar ion beam to remove any potential surface contamination. As shown in Fig. 4a, peak values at 1050.5 eV, 1027.4 eV, 730.7 eV, 719.9 eV, 535.6 eV, and 285.8 eV of binding energies could be indexed to the binding energy of Zn $2p_{1/2}$, Zn $2p_{3/2}$, Fe $2p_{1/2}$, Fe $2p_{3/2}$, O 1s, and C 1s, respectively, which confirmed the existence of Zn, Fe and O elements in the sample. Except them, the Eu 4d signal also was detected from the sample, indicating that Eu^{3+} ions maybe incorporated into the $ZnFe_2O_4$ successfully. We would like to mention that, for all the XPS spectra in Fig. 4, the binding energies had been calibrated by taking the carbon C 1s peak (285.0 eV) as reference. Fig. 4b, c, d and e were the high resolution scans of Zn 2p, Fe 2p, O 1s and Eu 3d of

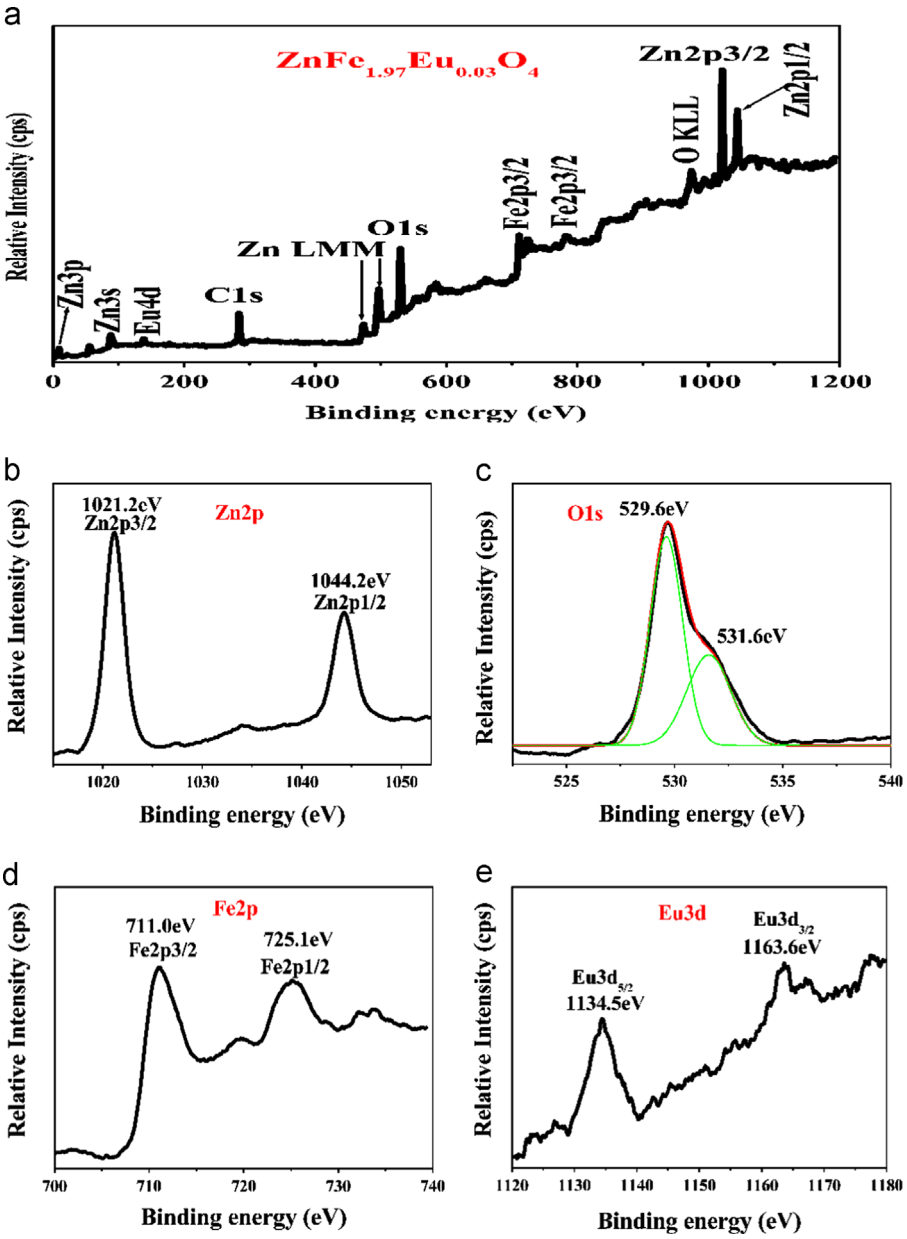

Fig. 4. XPS spectrum of $ZnFe_{1.97}Eu_{0.03}O_4$ nanoparticles: (a) XPS survey spectrum; (b) Zn $2p_{3/2}$ and Zn $2p_{1/2}$ XPS spectrum; (c) O1s XPS spectrum where two components (green curves) were used to deconvolute the experimental peak; (d) Fe $2p_{3/2}$ and Fe $2p_{1/2}$ XPS spectrum; (e) Eu $3d_{5/2}$ and Eu $3d_{3/2}$ XPS spectrum. (For interpretation of the references to color in this figure legend, the reader is referred to the web version of this article.)

$ZnFe_{1.97}Eu_{0.03}O_4$, respectively. For the Zn 2p XPS spectra shown in Fig. 4b, the peak located at 1021.2 and 1044.2 eV were associated to the $Zn2p_{3/2}$ and $Zn2p_{1/2}$, respectively, which could be assigned to two possible contributions, such as ZnO or spinel [9]. The spin orbit splitting of 23 eV indicates that the ion valence state is Zn^{2+} [10]. Since two oxygen species were obviously present in the O 1s XPS spectrum as observed in Fig. 4c, we fitted the spectra with Gaussian function and the deconvolutions showed the presence of two different O 1s peaks in the $ZnFe_{1.97}Eu_{0.03}O_4$ sample. The energy peak located at 529.6 eV was corresponding to the lattice oxygen, while the energy peak located at 531.6 eV was corresponding to the non-lattice oxygen (included adsorbed oxygen and oxygen in amorphous $ZnFe_2O_4$) [11,12]. The binding energy of Fe 2p was detected at 711.0 and 725.1 eV, which could be assigned to Fe $2p_{1/2}$ and Fe $2p_{3/2}$, respectively, only indicating the presence of Fe^{3+} cations [13]. Fig. 4d presents the Eu 3d XPS spectra of $ZnFe_{1.97}Eu_{0.03}O_4$. The two characteristic peaks at 1163.6 and 1134.5 eV were attributable to the core levels of Eu $3d_{3/2}$ and Eu $3d_{5/2}$, respectively, which indicated the Eu ions with trivalent incorporated into $ZnFe_2O_4$ lattices and substituted for the sites of Fe ions.

To investigate the magnetic properties of $ZnFe_{2-x}Eu_xO_4$ nanoparticles, their hysteresis loops were measured by VSM. Fig. 5 shows their magnetization curves. Typical "S"-like shape of hysteresis loops were observed, indicating a superparamagnetic property of the obtained samples. This superparamagnetic property

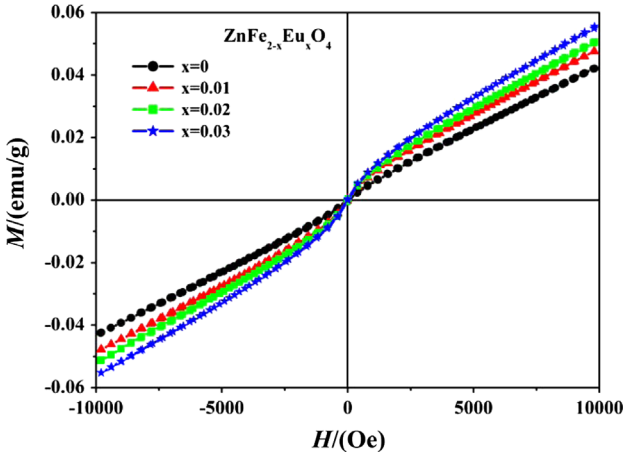

Fig. 5. Magnetic hysteresis loops of the $ZnFe_{2-x}Eu_xO_4$ ($0 \le x \le 0.03$) nanoparticles.

was evident by zero coercivity and remanence on the magnetization loop [14–17]. These "S"-like shape loops could be divided into two parts: curves and lines. The lines were attributed to the antiferromagnetic parts of the samples, and the curves might be ascribed to the change of the inversion parameter with the particle size decreasing to nanoscale, which was induced by the preparation techniques [18]. Moreover, we found that the hysteresis loops of the obtained nanocrystalline $ZnFe_{2-x}Eu_xO_4$ nanoparticles could not be saturated with the available maximum field of 10 kOe, indicating the presence of large anisotropy in the material. As shown in the figure, the M/H of the samples kept increasing with the increase of Eu^{3+} doping concentration [19]. For $ZnFe_{2-x}Eu_xO_4$ ($x=0$, 0.01, 0.02, 0.03) nanoparticles, the magnetization was 42 memu/g, 48 memu/g, 51 memu/g and 58 memu/g, respectively. According to Miller's site preference energies of ions [20], the cations distribution could be written as follows:

$$(Zn)[Fe_{2-x}Eu_x]O_4.$$

$$(A)(B)$$

According to the Neel model, the magnetic moment of $ZnFe_{2-x}Eu_xO_4$ ($x=0$, 0.01, 0.02, 0.03) nanoparticles was calculated by the following equation:

$$M = \left|M_B - M_A\right| = \left|6 - 2x\right| \quad (2)$$

where M_A and M_B are the magnetic moments in the A and B sites, respectively. Simultaneously, the term of saturation magnetization (M_s) was defined as the vector sum of magnetic moment per unit cell, and was written as the following equation:

$$M_s = \frac{8M}{a^3} \quad (3)$$

Thus, according to Eqs. (1) and (2), and the variations of lattices parameters a with Eu^{3+} doping concentration as discussed in XRD part, M_s should be decreased. But, it contradicted with the variation tendency of M_s in our case as shown in Fig. 5. Actually, the magnetic properties of ferrites were influenced by many factors, including the structure, composition, defects, and internal stress. Therefore, in our case, maybe we could use the following mechanism to explain the magnetic phenomena. On one hand, antiparallel Fe^{3+} ions in B site decreased with the increased of Eu^{3+} substitution, and the magnetic moments of Fe^{3+} ion was bigger than Eu^{3+} ion, which made M_B increase. On the other hand, the value of magnetocrystalline anisotropy constant (K_1) of Eu^{3+} ion was positive, those of Zn ferrites was negative. The incorporation of Eu^{3+} into Zn ferrites would result in the compensation of negative and positive value, and finally made $K_1 \to 0$, which meant the magnetocrystalline field reached the minimum. So, M_s gradually increased with the increase of Eu^{3+} doping concentration [21].

4. Conclusions

In this work, we synthesized Eu^{3+}-doped $ZnFe_2O_4$ nanoparticles by sol–gel method for the first time as we know. The detailed result revealed the $ZnFe_{2-x}Eu_xO_4$ ($x=0$, 0.01, 0.02, 0.03) nanoparticles had zero coercivity with the increasing M/H as the content of Eu^{3+} ions increased. Our results not only provide a candidate material for magnetocaloric applications, but inspire people to deeply investigate the rare-earth doped $ZnFe_2O_4$ nanoparticles in both theoretical and experimental aspects.

Acknowledgments

The authors would like to acknowledge financial support for this work from the National Nature Science Foundation of China (Grant nos. 11204104, 61178074, 61008051 and 11254001), Program for the Development of Science and Technology of Jilin Province (Item nos. 20110415, 201115219 and 20100113), Program for the Master Students' Scientific and Innovative Research of Jilin Normal University (Item nos. 201112, 201101 and 201139).

References

[1] M. Maletin, E.G. Moshopoulou, A.G. Kontos, E. Devlin, A. Delimitis, V.T. Zaspalis, L. Nalbandian, V.V. Srdic, Synthesis and structural characterization of In-doped $ZnFe_2O_4$ nanoparticles, Journal of the European Ceramic Society 27 (2007) 4391–4394.

[2] S. Urcia-Romero, O. Perales-Pérez, G. Gutiérrez, Effect of Dy-doping on the structural and magnetic properties of Co–Zn ferrite nanocrystals for magnetocaloric applications, Journal of Applied Physics 107 (2010) 09A508.

[3] J. Jensen, A. Mackintosh, Rare Earth Magnetism—Structures and Ex-citations, Oxford, Clarendon, 1991.

[4] M.H. Mahmoud, A.A. Sattar, Mössbauer study of Cu–Zn ferrite substituted with rare earth ions, Journal of Magnetism and Magnetic Materials 277 (2004) 101.

[5] Periodic Table of the Elements, Nach Fluck und Heumann unter Berücksichtigung der IUPAC-Empfehlungen bis 1987 (VCH Verlagsgesellschaft, 1988).

[6] J. Kong, F. Zhou, Z. Wang, C. Wang, M. Wang, K. Chen, X. Wu, K. Zhu, J. Qiu, Preparation and optical properties of high-quality oriented of Al and Er co-doped ZnO thin films, Journal of Sol–Gel Science and Technology 63 (2012) 95–102.

[7] A.K. Zak, R. Yousefi, W.H. Abd Majid, M.R. Muhamad, Facile synthesis and X-ray peak broadening studies of Zn_1–xMg_xO nanoparticles, Ceramics International 38 (2012) 2059–2064.

[8] R. Yousefi, A.K. Zak, F. Jamali-Sheini, The effect of group-I elements on the structural and optical properties of ZnO nanoparticles, Ceramics International 39 (2013) 1371–1377.
[9] A.C. Heredia, M.I. Oliva, C.I. Zandalazini, U.A. Agú, G.A. Eimer, S.G. Casuscelli, E.R. Herrero, C.F. Pérez, M.E. Crivello, Synthesis, characterization, and catalytic behavior of Mg–Al–Zn–Fe mixed oxides from precursors layered double hydroxide, Industrial & Engineering Chemistry Research 50 (2011) 6695–6703.
[10] G.E. Muilenbenger (Ed.), Handbook of X-Ray Photoelectron Spectroscopy, Perkin-Elmer Corporation, Minnesota, 1979.
[11] A.B. Djurisic, Y.H. Leung, K.H. Tam, Y.F. Hsu, L. Ding, W.K. Ge, Y.C. Zhong, K.S. Wong, W.K. Chan, H.L. Tam, K.W. Cheah, W.M. Kwok, D.L. Phillips, Defect emissions in ZnO nanostructures, Nanotechnology 18 (2007) 095702–095709.
[12] F. Jamali-Sheini, R. Yousefi, K.R. Patil, Surface characterization of Au–ZnO nanowire films, Ceramics International. 38 (2012) 6665–6670.
[13] L. Liu, G. Zhang, L. Wang, T. Huang, L. Qin, Highly active S-modified $ZnFe_2O_4$ heterogeneous catalyst and its photo–fenton behavior under UV–visible irradiation, Industrial & Engineering Chemistry Research 50 (2011) 7219–7227.
[14] F.S. Li, H.B. Wang, L. Wang, J.B. Wang, Magnetic properties of $ZnFe_2O_4$ nanoparticles produced by a low-temperature solid-state reaction method, Journal of Magnetism and Magnetic Materials 309 (2007) 295.
[15] F. Grasset, N. Labhsetwar, D. Li, D.C. Park, N. Saito, H. Haneda, O. Cador, T. Roisnel, S. Mornet, E. Duguet, J. Portier, J. Etourneau, Synthesis and magnetic characterization of zinc ferrite nanoparticles with different environments: powder, colloidal solution, and zinc ferrite–silica core–shell nanoparticles, Langmuir 18 (2002) 8209.
[16] J.F. Hochepied, P. Bonville, M.P. Pileni, Nonstoichiometric zinc ferrite nanocrystals: syntheses and unusual magnetic properties, Journal of Physical Chemistry B 104 (2000) 905.
[17] M.K. Roy, H.C. Verma, Magnetization anomalies of nanosize zinc ferrite particles prepared using electrodeposition, Journal of Magnetism and Magnetic Materials 306 (2006) 98.
[18] M. Wang, Z. Ai, L. Zhang, Generalized preparation of porous nanocrystalline $ZnFe_2O_4$ superstructures from zinc ferrioxalate precursor and its superparamagnetic property, Journal of Physical Chemistry C 112 (2008) 13163–13170.
[19] A. Khorsand Zak, W.H. Abd Majid, M. Ebrahimizadeh Abrishami, R. Yousefi, R. Parvizi, Synthesis, magnetic properties and X-ray analysis of $Zn_{0.97\times0.03}O$ nanoparticles (X=Mn, Ni, and Co) using Scherrer and size-strain plot methods, Solid State Sciences 14 (2012) 488–494.
[20] A. Miller, Distribution of cations in spinels, Journal of Applied Physics 30 (1959) 24S.
[21] L. Li, L. Peng, Y. Li, X. Zhu, Structure and magnetic properties of co-substituted NiZn ferrite thin films synthesized by the sol–gel process, Journal of Magnetism and Magnetic Materials 324 (2012) 60–62.